学位申請論文

大谷 浩

主論文

Radiative Cooling in the Intermediate Zone of a Shock Wave and its Effect on the Optical Emission Spectra of Supernova Remnants

Hiroshi Ohtani

Department of Astronomy, University of Kyoto, Kyoto, 606

Abstract

The temperature relaxation between electrons and heavy particles in the postshock gas is taken into consideration in the calculations of the structures of the shock waves runing into the gas in which hydrogen is partially preionized. A quick rise of the electron temperature at the immediate postshock region is followed by a rather gradual rise because of the inelastic collisions of the electrons with the hydrogen atoms. During the process of the temperature relaxation, the radiation loss due to the excitation of hydrogen exceeds the ionization loss. As the result, the maximum electron temperature is so low that a 100 km/sec model shock produces a spectral signature in the ultraviolet lines and the visual forbidden lines for shocks of 70 to 80 km/sec with hydrogen fully preionized. The electron temperature in the relaxation region is too high to excite the visual and infrared forbidden lines. On the other hand, the Balmer line emissions suffer some enhancement in Hα by the excitations during the temperature relaxation, and the resulting decrement shows a composite feature of the recombination decrement and the collisional decrement. A steep decrement seen in a filament of Vela X seems due to this cause.

Finally, a method of observation is proposed for the direct confirmation of the present results.

Key words: Shock wave; Temperature relaxation; Supernova remnant; shock spectra; Balmer Decrement.

1. Introduction

The earlier suggestions of the shock heating of the optical filaments of supernova remnants (Pikel'ner 1954, Parker 1964, 1967) were confirmed theoretically first by Cox (1972) who showed a satisfying agreement between the observed spectra in the Cygnus Loop and the ones calculated with the assumption of the establishment of the ionization equilibrium just behind the shock front. Later, calculating the ionization development from the immediate postshock region down to the final recombination zone, Dopita (1976, 1977) calculated shock spectra for various model waves to present the diagnostic diagrams for estimation of the elemental abundances from observed spectra of supernova remnants (Dopita et al 1977).

In his calculations, as well as in Cox's (1972), the full preionization model is assumed in which the preshock gas is so ionized that hydrogen and also elements with ionization potentials nearly same to that of hydrogen are fully ionized. However, he himself pointed out that the ultraviolet radiation produced in the postshock region is insufficient to ionize the preshock gas contrary to the model assumed. A very recent study by Raymond (1979) on the interstellar shock structure and spectra treats in detail the ionization and recombination for wide varieties of the shock velocity, the chemical composition and the preionization of the gas. For

the preionization, however, the ionization of hydrogen is taken essentially as to be fully ionized. There has been presented very recently another work (Shull and McKee 1979), in which the preionization has been calculated consistently to the ultraviolet flux produced in the postshock region. Here, the transfer of the ultraviolet radiation is treated with special attention, so that shocks faster than 110 km/sec have been found to ionize completely hydrogen and helium in their preshock gas.

There is an assumption common in models of the previous authors (Cox 1972, Dopita 1976, 1977, Raymond 1979, Shull and McKee 1979) that the equipartition of the thermal energy between the electron gas and the heavy particle gas is set up instantaneously at the immediate postshock region. However, it can be expected that the radiation loss during the process of the temperature relaxation can affect the visual spectral features, because the electrons successively heated behind the shock front experience temperature appropriate to the excitation of the visual lines.

In this regard, the temperature relaxation between the heavy particle gas and the electron gas were taken into consideration by Pikel'ner (1954) in his pioneering work on the shock spectra. He, however, neglected the effect of the compression of the shocked gas due to the radiative cooling and that of the precursor radiation. An analogous computation, but with the hydrodynamical effect being roughly taken into acount, was presented later by Bychkov (1973) for the purpose of explaining the coexistence of the X-ray and the coronal lines with the prominent optical emissions in the Cygnus Loop. He, however, took as a model for preionization that hydrogen and helium are completely and singly ionized, respectively, since he considered the intersection of two shock waves as supposed by Pikel'ner (1954).

Apart from the studies applied to real supernova remnants, the problem

at the immediate post shock region is discussed by Kaplan and Pikel'ner (1970) with aid of the results of somewhat sophisticated calculations of the interstellar shock structure (Podstrigach 1965, Kaplan and Podstrigach 1965). They argue that the radiative cooling before the temperature relaxation is important for shocks slower than 100 to 300 km/sec.

Therefore, we have calculated the shock structures and the emission spectra taking into account the temperature relaxation at the immediate post-shock region. However, our model calculations lack variety and treat the atomic processes and the radiative transfer in less detail than works of Raymond (1979) and of Shull and McKee (1979) which appeared after the previous manuscript of the present article was finished. We will confine ourselves to showing here our method, the resulting importance of the temperature relaxation and its effects on the shock structure and the visual spectra, putting aside the details of our results not pertaining to the temperature relaxation problem.

2. The Rankin-Hugoniot Relations

In order to calculate the shock structure with particular consideration of the relaxation process in the post shock region, it is important to see first how the gas is disturbed by the precursor radiation and later by the shock front itself. Therefore, before we examine the relaxation process itself, we consider the Rankin-Hugoniot relations and their solutions appropriate to the situation of the present study.

In addition to the basic fluid dynamical parameters, the ionization, the radiation flux and the magnetic field pressure should be introduced for the interstellar gas. In the following, physical parameters of gas are

normalized, similarly to Skalafuris (1965), in units of following values, respectively,

Particle number density: N_0 = undisturbed gas value, (1)

Velocity : $U_s = \sqrt{I_H/m_H} = 36.06$ km/sec, (2)

temperature : $T_s = I_H/K = 157745$ K, (3)

Alfvén velocity : $A_s = \sqrt{2}\, U_s$, (4)

radiation flux : $F_s = N_0 U_s I_H$, (5)

where I_H, m_H and k are the ionization potential of hydrogen atom, its mass and the Boltzman constant, respectively.

2a. The Equations and the Classification of the Solutions.

Across a control surface perpendicular to a plane parallel flow, density R, velocity v, temperature θ, Alfvén velocity a and radiation flux F, which are nondimensional quantities normalized by the above units, change according to the following Rankin-Hugoniot relations:

$$Rv = R_0 v_0, \tag{6}$$

$$R\{(1+\alpha)\theta + \mu v^2 + \mu a^2\} = R_0\{(1+\alpha_0)\theta_0 + \mu v_0^2 + \mu a_0^2\}, \tag{7}$$

$$\frac{\gamma}{\gamma-1}(1+\alpha)\theta + \frac{1}{2}\mu v^2 + 2\mu a^2 + \sum_{Z,z} X_{Z,z}\, \varepsilon_{Z,z-1}\alpha_{Z,z-1} - F$$

$$= \frac{\gamma}{\gamma-1}(1+\alpha_0)\theta_0 + \frac{1}{2}\mu v_0^2 + 2\mu a_0^2 + \sum_{Z,z} X_{Z,z}\, \varepsilon_{Z,z-1}\alpha_{Z,z-1,0} - F_0, \tag{8}$$

and to the equation of magnetic flux conservation:

$$a^2 v = a_0^2 v_0, \tag{9}$$

where the initial state is denoted by suffix 0, α is the concentration of

electrons relative to that of all heavy particles, γ the ratio of specific heats for monoatomic gas, i.e., $\gamma = 5/3$, μ the mean molecular weight of the gas in its neutral state, X_Z designates the fraction in number of an element Z, and $I_{Z,z}$ and $\alpha_{Z,Z}$ stand for the ionization potential in unit of I_H and for the ionization degree of the z times ionized ion of an element Z, respectively. The sign of the radiation flux is taken as positive for the upstream direction.

In the energy equation (8), the effect of the heat conduction is neglected. Therefore, our results obtained later are valid only when the angle between the magnetic field and the direction of flow is larger than a few tens degree (Raymond 1976).

These equations can be reduced into a cubic regarding to the reciprocal of the density jump:

$$\eta = R_0/R, \tag{10}$$

as

$$\eta^3 + p\eta^2 + q\eta + r = 0, \tag{11}$$

where

$$p = -\frac{2\gamma}{\gamma+1}\frac{1}{\mu v_0^2}\{(1+\alpha_0)\theta_0 + \mu v_0^2 + \mu a_0^2\} \tag{12}$$

$$q = \frac{2(\gamma-1)}{\gamma+1}\frac{1}{\mu v_0^2}\{\frac{\gamma}{\gamma-1}(1+\alpha_0)\theta_0 + \frac{1}{2}\mu v_0^2 + 2\mu a_0^2 + \sum_{Z,z} X_Z \mathcal{I}_{Z,z-1}(\alpha_{Z,z,0} - \alpha_{Z,z}) - (F_0 - F)\}, \tag{13}$$

and

$$r = \frac{2(2-\gamma)}{\gamma-1}\frac{a_0^2}{v_0^2} \tag{14}$$

Similar cubics were derived previously (Laan 1962, Cox 1972), but the present one is generalized to be applicable for arbitrary changes both in the ionization and the radiation field, whose effects are represented by the last two terms of (13).

Once the physical state of the upstream gas is given together with the changes of the ionizations and the radiation flux across the control surface, it is trivial mathematically to solve equation (11) and successively to find the unknowns using the equations in order of (10), (6), (9) and (7), as

$$R = R_0/\eta, \tag{15}$$

$$v = v_0\eta, \tag{16}$$

$$a = a_0/\sqrt{\eta}, \tag{17}$$

and

$$\theta = \frac{1}{1+\alpha}\mu v_0^2\eta\left\{\frac{(1+\alpha_0)\theta_0}{\mu v_0^2} + (1 - \eta) + (1 - 1/\eta^2)(a_0^2/v_0^2)\right\}. \tag{18}$$

However, amongst three solutions of the cubic equation, one must specify the one appropriate to the problem under consideration. Since the righthand sides of equations (12) and (14) are negative and positive, respectively, equation (11) has one negative and two positive solutions when

it has any positive solution. The smaller of the positives is always smaller than one, i.e., it denotes the compression of gas. Further, as this solution lies between $(\gamma - 1)/(\gamma + 1)$ and 1 if the last two temrs of (13) are omitted, we can identify this as the solution for shock discontinuity.

As to the other positive solution, it is independent of the value of the streaming velocity but depends only upon the changes of the ionization energy and of the radiation field whether the gas is rarefied or compressed. That is, the flow energy is not thermalized in the flow. Therefore, this solution is applicable to change of the physical state of interstellar gas when it is exposed to the precursor radiation from the postshock region, analogously to the considerations for the non-magnetic cases (Whitney and Skalafuris 1963, Skalafuris 1968, Narita 1973). The treaty given here should be coupled, in principle, with the result given by Shull and Mckee (1979) for the ionization ftructure of the preshock region.

2b. The temperature Separation

If a gas consists of two or more kinds of particle and their temperature are different from one another the temperature θ so far mentioned stands for the mean temperature of the gas. When interstellar gas ahead of a shock front is exposed to the precursor radiation from the postshock region, the temperatures are different in principle. However, it is found later to be unneccessary to consider this problem for the shock models considered in this study.

It is, however, important in the process of the thermalization of the flow energy at the shock front. We approximate the gas as composed of only two gas components, the electron gas and the heavy particle gas, since the temperature of atomic hydrogen is closely connected to that of proton through

mutual charge exchange in the post shock region (Skalafuris 1965) and also rapid interactions are expected among these particles and the other heavy particles, whose abundances are so small as never to be likely to affect the shock wave properties practically if any temperature differences existed.

At a shock front of a gas consisting of two kinds of particles with different masses, the relaxation time for the energy exchange between the different component is longer by a factor of the mass ratio of the heavier particle to the lighter than both time scales for relaxation among particles of same species when the rates of the three kinds of collision are same (e.g., Stupochenko et al. 1968). Therefore, whether the dominant component of the heavy particles of a gas is atomic hydrogen or protons, the thermal relaxation time between electrons and the major heavy particles is much longer than that within the heavy component itself and also than that within the electrons themselves. Thus, the temperature separation occurs between two kind of the gas component, since the flow energy of each component is proportional to its mass. This two fluid model composed of the heavy particles and electrons is more realistic than the two fluid model composed of the charged particles and neutral particles (Raymond 1976, Dopita 1978), since the charge exchange process is not considered in the latter model as pointed out by Raymond (1979).

Although the above consideration for a simple gas shock might be inapplicable straightforwardly to the interstellar medium, it is thought that any collisionless process is not dominant for shocks slower than 1000 km/sec or so (e.g., Kaplan and Pikel'ner 1970), and a possiblity of the temperature separation is pointed out in even faster shocks (Itoh 1978).

Therefore, we can assume in the present study that there is no appre-

ciable energy exchange between the electron gas and heavy particle gas within the shock front. Then, the energy conservation equation of the Rankin-Hugoniot relations holds separately for each gas component. At the shock front, the ionization of gas and its interaction with the radiation field can be neglected so that the following equation holds for the electron component;

$$\frac{\gamma}{\gamma-1}\alpha_0\theta_0 + \frac{\delta}{2}\alpha_0 v^2 + 2\delta\alpha_0 a^2 = \frac{\gamma}{\gamma-1}\alpha_0\theta_{e,0} + \frac{\delta}{2}\alpha_0 v_0^2 + 2\delta_0 a_0^2, \tag{19}$$

where θ_e is the electron temperature, and δ is the mass ratio of electron to hydrogen atom. In this equation, the energy of the magnetic field is assumed to be associated proportionally to the mass density of each gas component. Applying η so specified appropriate to the shock discontinuity as mentioned above to (19), one finds the electron temperature at the immediate postshock region as

$$\theta_e = \theta_{e,0} + \frac{\gamma-1}{\gamma}\{\frac{\delta}{2}v_0^2(1-\eta^2) + 2\delta a_0^2(1-1/\eta)\}. \tag{20}$$

For the heavy particle gas component, an equation analoguous to (19) holds. It is, however, unnecessary to solve it explicity, because one can derive the heavy particle temperature θ_h from a simple equation of the definition of the mean temperature of gas θ;

$$(1+\alpha)\theta = \theta_h + \alpha\theta_e, \tag{21}$$

θ, θ_e and α being known quantities.

3. The method of the Calculation

3a. The outline

The first step of the calculation is to obtain the physical state of the precursor gas just in front of the shock front. Assuming no recombination in the preshock region and neglecting the absorption of the radiation by species other than hydrogen atom, one can find that the increase of the number of the ionized hydrogen due to the precursor radiation is equal to the photon flux of the ionizing photons, i.e., $\alpha_{HII} = \mathcal{F}_H$ for $\mathcal{F}_H < 1$, $\alpha_{HII} = 1$ for $\mathcal{F}_H \geq 1$, $\mathcal{F}_H$ being the photon flux normalized by $X_H N_0 U_s$. The photon flux together with the energy flux is given by the calculation of the postshock region mentioned later. As for the ionizations of the other elements in the preshock gas, C, N, O, Mg, Si and S have been assumed to be ionized as well as hydrogen. Furthermore, we have assumed the radiation loss from the precursor gas to be negligible.

Then, the immediate preshock state can be found from the Rankin-Hugoniot relations as mentioned in the previous section. In succession, the result is again put into the relations to determine the physical parameters, including θ_e and θ_h, of the gas just behind the shock front.

Once the immediate postshock state is obtained, changes of the various physical quantities can be traced downstream similarly to the earlier works (Cox 1972, Dopita 1977, Raymond 1979, Shull and Mckee 1979). There is, however, an essential difference in our procedure from theirs that the integration of the energy equation regarding the electron gas is included in

addition to that of the equation for the whole gas component.

For the whole gas, by introducing enthalpy per particle (the particle includes its associated free electrons), H:

$$H = \frac{\gamma}{\gamma-1}(1 + \alpha)\theta + \frac{1}{2}\mu v^2 + 2\mu a^2, \tag{22}$$

one can write the energy equation as

$$\frac{dH}{dx} = -\sum_{Z,z} X_Z z\ell_{Z,z-1}\frac{d\alpha_{Z,z}}{dx} + X_H\frac{dF_H}{dx} + \frac{dF_c}{dx} \tag{23}$$

for a plane-parallel stationary flow, where the distance x is measured downstream from the shock front. The effect of radiation is represented separately for the simple radiative cooling, dF_c/dx, and for the heating and cooling through hydrogen, $X_H dF_H/dx$, where F_H is the energy flux per hydrogen, i.e., the flux normalized by $X_H F_s$.

Similarly, as for electron gas, with a notation H_e, the enthalpy per free electron:

$$H_e = \frac{\gamma}{\gamma-1}\theta_e + \frac{\delta}{2}v^2 + 2\delta a^2, \tag{24}$$

the energy equation can be written as

$$\alpha\frac{dH_e}{dx} = G - \sum_{Z,z} X_Z z\ell_{Z,z-1}\frac{d\alpha_{Z,z}}{dx} + X_H\frac{dF_H}{dx} + \frac{dF_c}{dx} + \frac{\delta}{\mu}H_h\frac{d\alpha}{dx} - H_e\frac{d\alpha}{dx} \tag{25}$$

where G stands for the energy transfer from the heavy particles through

elastic collisions, and the term including H_h, enthalpy associated to a heavy particle, shows the rate of enthalpy shared to the electron gas or added to the heavy particle gas in the ionization or recombination, respectively. The last term denotes the direct effect of the change of the electron concentration. We note that the net change of the enthalpy of the whole gas can be approximated as being wholly attributed to the electron gas as seen in equation (22) and (24), since the energy change of a heavy particle concerned to these processes is negligibly small because of its massiveness compared with an electron. Thus, the heavy particles are cooled only through energy transfer to electrons.

Equations (23) and (24) should be supplemented by ionization equations for each species, the radiative transfer equations for the ionizing radiation and the equation for the radiative cooling. The ionization equations used are the ordinary nonstationary ones including both collisional and radiative processes (e.g., Dopita 1976), and the radiative cooling is described in the next paragraph.

Concerning to the transfer equation of the Lymann continuum, in addition to the equation for the energy flux, the equation for the photon flux $\mathcal{F}_H$ was also considered to define the mean photon energy,

$$\epsilon = F_H/\mathcal{F}_H, \tag{26}$$

at each point, and the absorption coefficient was computed correspondingly to this photon energy. Both for F_H and $\mathcal{F}_H$ the Eddington two stream approximation were employed. For simplicity, the ionization and heating of the gas by absorbing ultraviolet lines were not treated in the calculation; the effect of this radiation on the result will be evaluated for each model computed.

To find θ_e from equation (25), the derivatives of v and a are also required. One can obtain them by differentiating equations (7) and (9) with the aid of equations (6) and (22) to eliminate θ and R;

$$\frac{dv}{dx} = \frac{1}{v}\left(\frac{dH}{dx}\right)/\left\{\frac{H}{v^2} - \frac{\gamma+1}{2(\gamma-1)}\mu + \frac{2(2-\gamma)}{(\gamma-1)}\mu\left(\frac{a^2}{v^2}\right)\right\}, \tag{27}$$

and

$$\frac{da}{dx} = -\frac{1}{2}\frac{a}{v}\frac{dv}{dx}. \tag{28}$$

In the practical procedure, the above two equations were used only to get θ_e, and were not integrated for v and a in order to avoid the accumlation of errors in the numerical calculation. To determine the hydrodynamical quantities, R, v, a and θ, the Rankin-Hugoniot relations were solved for each step end of the integration; H found from equation (23) was introduced into equation (13) instead of the factor parenthesized by the larger brackets. For θ_h, equation (21) was used. After the above procedures had been finished over the whole structure, the radiative transfer equations were integrated to find the radiation fields, which were adapted to the next iteration.

3b. Atomic parameters and Cooling Agents

The interaction of hydrogen with free electron consists of the elastic and inelastic processes. For the elastic collision, the energy transfer rates were employed from Skalafuris (1965) both for the atom-electron and the proton-electron collisions. The ionization and excitation coefficients were calculated by using the semiempirical formula by Kanno (see Itoh and Kogure 1967). The excitations up to the 20-th level were included in the

present calculation. For the free-bound and for free-free transitions, Seaton's (1959a, 1959b) coefficients were used not only for hydrogen but also for continuous emission rates of HeII and HeIII.

The elements other than hydrogen considered are He, C, N, O, Ne, Mg, Si, and S, whose abundances were taken according to Allen (1973). For these elements, the recombination rates were derived after Aldrovandi and Pequignot (1973, 1976), and the ionization and the permitted line excitation rates by electronic collision were computed from the formula by Cox and Tucker (1969), the atomic constants being taken from Cox (1970). Also, the constants for the forbidden lines were taken from him except for [S II], for which the data used are ones from Czyzak (1968). Further, semi-forbidden line excitations were considered for the transitions tabulated by Osterbrock (1970).

As for the radiative ionization, the ions whose ionization potentials are lower than or nearly same as that of hydrogen, i.e., CI, NI, OI, MgI, MgII, SiI, SiII and SI, were considered. The absorption coefficients were approximated simply as hydrogen-like with the threshould value equal to that of hydrogen.

4. The Numerical Results and Discussions

4a. The Shock Wave Structure

Numerical calculations were made for three shock velocities, 100, 140, and 170 km/sec. However, since the problem of the temperature relaxation is found to be less important in the latter two cases, we mainly discuss the results on the 100 km/sec shock. For all cases, the physical parameters of

the undisturbed interstellar medium were taken as follows. The density is 10^{-24} gcm^{-3} ($N_0 \simeq 0.43$ cm^{-3} or hydrogen concentration $\simeq 0.39$ cm^{-3}), the temperature is 100 K ($\theta \simeq 6 \times 10^{-4}$), and the ionization degrees are 10^{-3} for all elements considered except for He and Ne which are neutral. Further, the magnetic field strength is 2×10^{-7} gauss, and there is no radiation field.

We give the physical state of the immediate preshock gas in table 1. The gas is heated up to about 500 K and the hydrogen is ionized to about 10 percent by the precursor radiation $-F_H$. The mean photon energy is $\xi = 1.05$; this implies that the recombination of hydrogen occurs efficiently at the postshock region where the electron temperature is $\sim$5000 K.

table 1

Next, at the shock front the temperatures of electrons and heavy particles, T_e and T_h respectively, are separated as shown in the column designated as 'shock' in the table. The shock are strong enough to compress the gases up to the limit of 4 times and to heat heavy particles over 3×10^5 K. However, the temperature rise of electron gas is small compared with that of the heavy particle gas. This can be interpreted as the front not being supersonic for most electrons, because the mean kinetic velocity of the electrons passing into the front is $\sim$150 km/sec which exceeds the shock velocity.

The wave structure behind the front with velocity 100 km/sec is shown in figure 1. An remarkable feature is a very quick rise of T_e up to $\sim$50000 K within a very short distance 3×10^{14} cm, while T_h drops only a little and the ionization of hydrogen hardly developes. Thereafter, the tempera-

ture rise of the electrons turns into a rather gradual one until the relaxation between T_e and T_h is nearly established as $T_e = T_h = T = 9 \times 10^4$ K at a distance of 6×10^{15} cm, where hydrogen becomes fully ionized. The physical parameters of the gas there are given in the last column of table 1.

figure 1

figure 2

Figure 2 shows the rates of change of the enthalpy H_e per electron through various processes. It can be seen from the figure that the very quick rise of T_e at the beginning is caused by the energy transfer from protons. This quick heating is blocked by the onset of the energy loss due to the excitation and ionization of hydrogen, and by the resultant increase of the number of free electrons which can obtain little excess energy when they are detatched from the parent atoms. Meanwhile, the increase of the density of protons, which results partly from the ionization itself and partly from the compression of the gas by the expenditure of the thermal energy on the inelastic collisions, makes the electron-photon elastic collisions frequent enough to activate again the heating of the electrons. Thus, the relaxation between T_e and T_h and the complete ionization of hydrogen occur nearly simultaneously. The heating and ionization by the radiation is of little importance in the relaxation region, since its opacity for Lyman continuum is so small that the radiation is hardly absorbed as is shown in figure 1.

It is important to notice, as seen also from figure 2, that an appreci-

able fraction of the electron energy expended on the inelastic collisions during the temperature relaxation process is due to the excitation of hydrogen atoms. The amount of the excitation energy can be known as the difference in the quantity $E = H + X_H \alpha_{HII} + X_{He} \mathscr{E}_{HeI} \alpha_{HeII} - X_H F_H$, the total energy per particle, between 'shock' and 'relaxation' states in table 1. The difference is found to be $\Delta E = 1.47$. Further, it should be noticed that the excitation loss ΔE greatly exceeds the ionization loss which is equal to $X_H + X_{He} \mathscr{E}_{HeI} \alpha_{HeII} \simeq 0.9$. This comes from the fact that an atom suffers the ionizing collision only once before the establishment of the temperature relaxation while the excitation occurs more than once; for a typical physical state of the gas under the relaxation process, $\alpha_{HII} \simeq 0.6$, $N_e \simeq 1\ cm^{-3}$ and $T_e \simeq 7 \times 10^4$ K, the recombination time $\sim 4 \times 10^{13}$ sec is found to be longer than the time interval required for a particle to reach the relaxation point, 3×10^9 sec, during which an atom is excited at a rate $3 \times 10^{-9}\ sec^{-1}$.

As to the ionization of the other elements, the ionization fractions of some elements are shown in figure 3 for the 100 km/sec model. With the increase of T_e, the ionizations develope rapidly as well as for hydrogen. When $T_e = T_h$ is established, most of Si and Mg and about half of S are doubly ionized while C, N and O are in singly ionized states. However, He and Ne are still mostly neutral.

figure 3

The above feature of the ionization states at the temperature relaxation point together with the temperature 9×10^4 K is almost same as that at

the immediate postshock state in Dopita's (1977) standard model or also that in Raymond's (1979) model D. These models give temperatures 1 x 10^5 K just behind a shock front moving at 81.5 km/sec into the preshock gas assumed to be ionized hydrogen and helium in its neutral state. Therefore, the shock structure of our 100 km/sec model further behind the temperature relaxation point is so analogous to their models that it is no longer necessary to describe except for a comment on the scale. After scaling their structures in proportion to the reciprocal of the preshock density ratio to our model, respectively, one finds that the structure obtained shows shorter scale than theirs; for example, the scale to the point where the temperature drops to 10000 K from the temperature relaxation point in our model is about a half of the scale to the same temprature from the shock front in model D of Raymond (1979). In our model, the compression of the gas is about eight times at the temperature relaxation point because of the radiation loss and the ionization loss, while the compression just behind the shock front is equal to the classical limit, i.e., four times in the fully preionized model. Therefore, the scale of our model is reduced by about twice compared with the Raymond's (1979) model.

4b. The Considerations on the Preshock Region

The ionizing radiation emitted upstream ionizes the undisturbed gas before it penetrates into the shock front. The effect on the results presented as far should be evaluated. In the process of the calculation of the strucrure the number and the energy of the photons radiated for each ionizing line were obtained. At most, a half of the photon can be assumed to flow back to the preshock region. Then, the photon flux for the presented model is found to be 0.32 per incoming hydrogen including the Lyman continuum tabulated in table 1. This estimation confirmed by the following

fact. That is, a shock of ∿85 km/sec is found to be able to preionize up to 0.3 from figure 5 of Shull and Mckee (1979), while the difference in kinetic energy of gas penetrating into the shock front is 1.5 I_H per particle of $\mu = 1.377$ between 100 km/sec and 85 km/sec shocks. In their model, the excitation loss seems to be of little importance since the electron temperature at the immediate post shock region is so high that the ionization rate greatly exceeds the excitation rate there. Therefore, the energy difference is consistent with the radiation loss $\Delta E = 1.47$ during the temperature relaxation in our 100 km/sec model as obtained above. The preshock gas is, therefore, ionized up to a degree of ∿0.3 in the region up to 1×10^{17} cm ahead of the front which corresponds to a unit optical depth of the preionized gas for the precursor photon whose energy ϵ is 1.4 in average. The time required for the gas to reach the shock front is 10^{10} sec.

The ionizing photons are so energetic that the electrons detached from the hydrogen atoms are heated up to 25000 K which corresponds to $2(\epsilon - 1)/5$. The fastest kinetic process in the gas under this situation is found to be the energy exchange between electrons and protons; the temperature of the latter is still 100 K. The equilibrium temperature 5600 K found from equation (21) is established in a time scale of 1×10^{8} sec, which is evaluated from the equation: $d\theta/dt \simeq 3 \times 10^{-9} X_H N_0 \alpha_{HII} (\theta_0 - \theta_e) \theta_e^{-3/2}$. It can be seen that the gas suffers thereafter no appreciable change by the cooling, recombination and ionization until it meets the shock front.

The temperature of 5600 K is much higher than the preshock temperature 500 K obtained by ignoring the ultraviolet lines. However, the jump of the electron temperature is only 128 K which is same as that shown in table 1, because a quantity $\theta_e - \theta_{e,0}$ is found from equation (20) to be independent of $\theta_{e,0}$ for shocks as strong as $\eta = 1/4$. The electron the tempe-

rature at the immediate postshock region is, therefore, much lower than 50000 K at which the excitation of hydrogen begins as seen in the preceding subsection. In other shock models calculated for velocities 140 and 170 km/sec, the excitation of hydrogen becomes efficient at temperatures not so higher than 50000 K, the preionizations are 0.1 by Lyman continuum only, and the heavy particle temperatures are as high as 6×10^5 K and 9×10^5 K, respectively. Therefore, it is suggested that the heating effect of the preshock gas due to the precursor radiation is not so important for shocks in partially ionized gases if the temperature of the undisturbed gas is appreciably lower than 50000 K.

As for the effect of the degree of the preionization, the higher ionization degree implies a shorter time interval till the temperature relaxation is established in the postshock region, and also, of course, makes the ionization loss smaller. The energy loss due to excitation of hydrogen, however, seems not to be so severely affected by a small change of the initial ionization degree. As is seen in figure 1 and 2, the excitation dominates within a rather thin layer where hydrogen ionized to about 0.6. Also, in the 140 and 170 km/sec models, the feature is similar; the ionization degree of the layers where the excitation is efficient is 0.7 for both models although the electron temperatures are 1.0×10^5 K and 1.2×10^5 K, respectively.

From above considerations, the structure of the temperature relaxation region seems to similar to that in the model described in the previous subsection as long as the preionization is lower than 0.5 or so. In regard to this, the models with velocities 140 km/sec and 170 km/sec, however, produced ionizing precursor photons which amount respectively to 1.3 and 1.8 per hydrogen incoming, consistent to the argument of Shull and Mckee (1979). Since the preshock gas is completely ionized for these precursor fluxes, the

excitation loss before the temperature relaxation is no longer meaning full at least for hydrogen.

4c. The Ultraviolet Lines and the Forbidden Lines

In the process of the numerical integration for the shock structure, the energy losses due to excitations of permitted lines except for hydrogen and semiforbidden lines in each step of the integration have been accumulated over the whole structure of a shock wave for the respective lines. In table 2, the resulted 'spectra' are given for lines with the wavelengths longer than the Lyman threshold.

table 2

As expected from the structural similarity mentioned above of Raymond's (1979) model D to the part behind the temperature relaxation point of our 100 km/sec model, the spectral features of the two models are compatible each other. However, a closer comparison of our result to his with the same elemental abundances as ours reveals that his model C shows a better coincidence with our model rather than the model D. The spectra tabulated in the last column of table 1 are from Raymond (1979), the unit being reduced in I_H per incoming particle. Since the chemical composition adopted in his model C is same as that in the present calculation, we refer to his result for comparison of the spectral features rather than results by others (Dopita 1977, Shull and Mckee 1979). His model C with the shock speed 70.7 km/sec gives a gas temperature of 7×10^4 K just behind the front running into the preionized gas assuming hydrogen and helium to be ionized com-

pletely and singly, respectively. On the other hand, in our 100 km/sec model, the temperature is also 7×10^4 K at the point where helium becomes singly ionized as one can see from figures 1 and 3. A smaller fraction of the radiation given in table 2 is radiated from the region between the front and that point. Thus, the similarity in the ultraviolet spectra between the two models is found to be quite reasonable.

The structral similarity as above gives the general coincidence, at least, in the visual spectra of the forbidden lines as seen in table 3. The spectra have been calculated from the level populations obtained for the respective species by assuming the statistical equilibrium for the physical state at each step of the integration for the shock structure.

figure 4

table 3

The distributions of the emissivities of the lines originating in oxygen are illustrated in figure 4. As concerns [OIII]λ5007/4959, there arises no emission from the temperature-relaxation region since oxgen cannot be ionized twice there as is shown in figure 3. Although some contribution from the gas during the temperature-relaxation process is apparent in the figure for each line other than [OIII], the amount does not exceed 10 percent of the total emission even in the extreme case. Thus, the gas before the full ionization of hydrogen is too rare and the electrons in the gas are too hot to excite efficiently the visible and infrared forbidden lines.

Next, we should like to notice the relative intensities within nitrogen lines; the lines from the singly ionized ion are weaker in our model compared with the mode C of Raymond (1979) while the situation is reversed for the atomic line. This difference can be attributed partly to our ignoring the charge exchange between nitrogen and hydrogen, and partly to our rather crude assumption of ignoring the ionization by the ultraviolet lines. The assumption gives also underestimation of the photoionizations of CI, MgI, SiI and SI, in the cool region. Looking into more in detail the two results for the visual lines, we find the intensities from our model are somewhat weaker for most lines than those from the model being compared; the latter model emits more light by about 25 % than the former within the visual lines tabulated in table 3. This difference between the two models can be explained, as pointed out by Dopita (1977) as the effect of the hydrogen ionizing lines. These, being more important in their effect on the heating than on the ionization balance, strengthen the forbidden lines. Therefore, in contrast with the above, fairly stronger infrared emission resulted in our case than in Raymond's (1979) case.

Therefore, if we treated models where the heating and ionization by the ultraviolet lines were taken into consideration, the contribution to the total emission of any visual forbidden line from the recombination zone should in fact be somewhat larger than in the present calculation. On the otherhand, the situation is reversed for the fine structure lines, and, therefore, the relative importance of the contribution from the temperature relaxation region to the total amount of the emission should be greater than the present result. However, the contribution from the region can be found to be negligibly small in practice even if in the extreme where the one from the recombination zone is suppressed by 10 times, as seen from

figure 4. Thus, we are led to a conclusion that the postshock region just behind the shock front never affects the visual and infrared spectra of forbidden emissions in hydrogen-ionizing shock waves.

4d. The Balmer Decrement

In order to obtain the hydrogen line intensities, the statistical equilibrium among the level populations of a model atom with twenty discrete levels was assumed at every point of the postshock region. The relative distributions of the emissivities of Hα and Hβ computed for Case B are given in figure 5, where two distinct emission regions are seen for each line. The first region corresponds to the one where the temperature relaxation is progressing, and the second to the one of the recombination of hydrogen. In the former region the ionization state is so different from the equilibrium one that about forty percent of hydrogen is still neutral although the electron temperature is as high as 7×10^4 K at the point of the emission peak. Therefore the atomic levels are populated by extensive excitations and negligible recombinations. Extraordinarily large b_n values and a very steep decrement compared with the equilibrium collisional decrement for the same temperatures resulted, as is shown in the third column of table 4. On the other hand, the line emissions from the second region show essentially pure recombination spectra corresponding to the ones for the temperature there, as shown first by Cox (1972). The Balmer decrement at the emissivity peak where T = 5230 K and $\alpha_{HII} = 0.690$ is also tabulated in the fifth column of table 4.

figure 5

table 4

The hydrogen spectra from the whole postshock region were obtained both for Case A and Case B by integrating the emissivity of each line. The result for Case B is given in the last column of the same table. A conspicuous feature of the shock decrement is the large value of Hα/Hβ compared to the recombination case, while the higher members are close to the ones in recombination region. The contributions to the total emission from the first emission region are estimated be to about thirty and ten percent for Hα and Hβ, respectively. The resulting absolute intensity of Hβ is greater than the interpolated value of the recombination component for the shock producing the preionization 0.3 from the results of Shull and Mckee (1979).

The enhancement of Hα by the collisional excitations at the immediate post shock region in some models of Shull and Mckee (1979) is different from our case in the temperature of the exciting electrons; it is much lower in our model than in theirs since they assumed the one fluid model. In view of the excitation temperature of hydrogen atoms just behind the shock front, Dopita's (1978) models of shock waves in patially ionized gases with post-shock temperature 6×10^4 to 10^5 K are similar to our model. Therefore, Hα/Hβ ratios of shock spectra are also consistent between his result and ours. (The excitation rates used by him do not differ by more than 20 % from those used in the present calculation at Te = 7×10^4 K.) However, his model, the two fluid model of neutral particles and charged particles, is less realistic than our two fluid model of heavy particles and electrons, as mentioned in section 2.

However, in any case, the strong enhancement of Hα seems a theoretical extremity since the Case B assumption for the first region is found to be quite marginal. From the calculated shock structure, it can be estimated that the first layer is effectively a thin layer which is thick for Lyman photons emitted upstream but thin downstream. This comes from the steep increase of the ionization degree from the shock front toward the fully ionized region, and also comes partly from the high atomic temperature. A similar situation is expected in the high temperature part of the recombination region; this part seems transparent for Lyman lines toward the shock front.

From the above considerations, we have constructed model Balmer decrements on the basis of the calculated results in order to try to better represent real phenomena. The model assumes that a half of atoms in the temperature relaxation region is treated as Case A and other half is as Case B while in the recombination region the pure radiative Case B holds. The line intensity ratios were taken to be typical ones at the emission peak given in table 4 the first emission region. For the second region, the result for T_e = 5000 K and $N_e = 10^2$ by Brocklehurst (1971) was employed. We have used so far the recombination coefficients not allowing for the l-degeneracy (Seaton 1959b) to avoid a tremendous complication for calculating the level pupolations at each point in the wave taking into the effects of the collisional excitations. However, it has been already clear that the electron temperature in the first emission layer is so high as the populations can be infered from the results of Brocklehurst (1971) to be approximately distributed statistically wihtin l-states at least for lower level down to a low electron density at the first emission peak. Therefore, the model decrement is consistent from the point of view of the l-degeneracy.

figure 6

The resulting decrements down to Hδ are shown as log (Hα/Hβ) vs.log (Hγ/Hβ) and log (Hγ/Hβ) vs.log (Hδ/Hγ) in figure 6. The relative importance of the contribution from the temperature relaxation region to the total emission is taken as parametric in the fraction of Hβ to imitate different shock velocities; the contribution is the smaller for the slower shock. The radiative decrement for T_e = 5000 K reddened by the interstellar extinction is also shown. Although the reddened decrement mimics the shock decrement, the loci of the two kinds are further separated than in the case of Miller (1974) who allowed for the collisional excitation in the recombination region of the shock wave heating a preshock gas fully ionized.

In figure 6, also some observational results of quality are plotted. The decrements from Hα down to Hγ of the Cygnus Loop (Miller 1974) are well explained by the model decrement with negligible contribution from the temperature relaxation region since a reddening E_{B-V} = 0.08 is measured for this object (Parker 1964). The observational results for log (Hγ/Hβ) vs. log (Hδ/Hγ) are located too far from both theoretical predictions. This can be attributed to the possible observational errors in Hγ (Miller 1974). As for Vela X (only in figure 6a), the observational result (Osterbrock and Costero 1973) can be apparently interpreted as the reddened decrement with E_{B-V} = 1.7. However, the reddening of this supernova remnant appears to be negligible (Dopita et al. 1977), or a measured interstellar extinction is A_V = 0.3 (Milne 1968), that is E_{B-V} = 0.1. Further, the emission spectrum of the filament under consideration indicates a rather slow shock velocity; the immediate postshock temperature is estimated by Dopita et al (1977) as $7 \sim 8 \times 10^4$ K, i.e., ~80 km/sec, or about 70 km/sec is suggested by Raymond (1979). Both results are from models with full preionization. Therefore, we can expect some enhancement of Hα by the temperature relaxation region

for this filament. There is one more object for which the higher members of Balmer series over Hβ are observed. The object is N49 (Osterbrock and Dufour 1973). The observed decrement is, however, located in far upper left regions out of both figures 6a and b. Therefore, no interpretation can be found.

5. A Concluding Remark

In view of the difficulties in accurate measurements both of the line intensities and the reddening, a method of observation is advantageous for the direct confirmation of the contribution in Balmer lines from the just behind the shock front. The method is to measure the width of a filament image of a supernova remnant in an appropriate visual forbidden line and that in the 'pure Hα light' not contaminated by [NII] lines. Since the filament of supernova remnants are generally thought as 'edge-on-seen sheet' of the shock wave, a larger width in Hα than in forbidden line lines is expected for the object with extensive collisional excitation of hydrogen in the temperature relaxation region. For an object located at a distance of 1 Kpc, the angular extent for 1 second of arc corresponds to 1.5×10^{15} cm, while the distance from the first emission peak to the second is expected as to be $(3 \sim 4) \times 10^{15}$ cm for shocks with velocity $\lesssim$100 km/sec and preshock density 10 particle$\cdot$cm^{-3} from figure 5 togetherwith the consideration given in the previous section. Therefore, it seems rather easy to confirm qualitatively and even quantitative measurements can be expected for nearer objects.

I am very grateful to Professor T. Kogure for his leading in my study on the interstellar shock waves, and also to Professors T. Shimizu and Y. Ôno for their continuous encouragement. The author would like to thank Drs. M. A. Dopita and J. C. Raymond for their valuable comments and reading of the manuscript critically as the referees of this article.

The numerical calculations were carried out by using FACOM 230-60/75 at the Data Processing Centers of Kyoto University and of Hokkaido University.

References

Aldrovandi, S.M.V. and Pequinot, D. 1973, Astron. Astrophys., 25, 137.

Aldrovandi, S.M.V. and Pequinot, D. 1976, Astron. Astrophys., 47, 321.

Allen, C.W. 1973, Astrophysical Quantities (Athlon, London), p. 30.

Bychikov, K.V. 1973, Commun. Special Astrophys. Obs., No. 10, 3.

Cox, D.P. 1970, Ph. D. Dissertion, UCSD.

Cox, D.P. 1972, Astrophys. J., 178, 143.

Cox, D.P., and Tucker, W.H. 1969, Astrophys. J., 157, 1157.

Czyzak, S.J. 1968, in Nebular and Interstellar Matter, ed. B.M.Middlehurst and L.H.Aller (University of Chicago Press, Chicago), p. 403.

Dopita, M.A. 1976, Astrophys. J., 209, 395.

Dopita, M.A. 1977, Astrophys. J. Suppl. Ser., 33, 437.

Dopita, M.A. 1978, Astrophys. J. Suppl. Ser., 37, 117.

Dopita, M.A., Mathewson, D.S., and Ford, V.L. 1977, Astrophys. J., 214, 179.

Itoh, H. 1978, Publ. Astron. Soc. Japan, 30, 489.

Itoh, S., and Kogure, T. 1967, Mem. Coll. Sci., Univ. Kyoto, Ser. A, 31, 241.

Kaplan, S.A., and Pikel'ner, S.B. 1970, The Interstellar Matter, transl. M.Sreda (Harvard University Press, Cambridge), p. 208.

Kaplan, S.A., and Podstrigach, T.S. 1965, Soviet Astron., 9, 438.

Laan, H. van der. 1962, Monthly Notices Roy. Astron. Soc., 124, 125.

Miller, J.S. 1969, Astrophys. J., 157, 1215.

Milne, D.K. 1968, Australian J. Phys., 21, 201.

Narita, S. 1973, Prog. Theor. Phys., 49, 1911.

Osterbrock, D.E. 1970, in Nuclei of Galaxies, ed. D.J.K.O'Connell (North-Holland Publishing Co., Amsterdam). p. 151.

Osterbrock, D.E., and Costero, R. 1973, Astrophys. J. Letters, 184, 71.

Osterbrock, D.E., and Dufour, R.J. 1973, Astrophys. J., 185, 441.

Parker, R.N.R. 1964, Astrophys. J., 139, 493.

Parker, R.N.R. 1967, Astrophys. J., 149, 363.

Pikel'ner, S.B. 1954, Izv. Krimsk. Astrofiz. Obs., 12, 93.

Podstrigach, T.S. 1965, Ukr. Fiz. Zh., 5, 601.

Raymond, J.C. 1976, Ph. D. Dissertion, University of Wisconsin-Madison.

Raymond, J.C. 1979, Astrophys. J. Suppl., 39, 1.

Seaton, M.J. 1959a, Monthly Notices Roy. Astron. Soc., 119, 81.

Seaton, M.J. 1959b, Monthly Notices Roy. Astron. Soc., 119, 90.

Shull, J.M., and Mckee, C.F. 1979, Astrophys. J., 227, 131.

Skalafuris, A.J. 1965, Astrophys. J., 142, 352.

Skalafuris, A.J. 1968, Astrophys. Space Sci., 2, 258.

Whitney, C.A., and Skalafuris, A.J., Astrophys. J., 138, 200.

Table 1

The physical states of gas at the immediate preshock, the immediate postshock, and the temperature relaxation points (shock velocity = 100 km/sec, $\rho_0 = 1 \times 10^{-24} gcm^{-3}$, $\alpha_{HII, 0} = 10^{-3}$, $T_0 = 100$ K, $B_0 = 2 \times 10^{-7}$ gauss, $\mu = 1.377$)

parameter*	preshock	shock	relaxation
ρ	1×10^{-24}	3.99×10^{-24}	7.56×10^{-24}
T_h	-	313000	-
T	488	298000	90000
T_e	-	612	-
H	5.30	5.30	2.99
α_{HII}	0.0952	0.0952	1.00
α_{HeII}	0.0	0.0	0.20
$-F_H$	0.0988	0.0988	0.106

* For notations, see text.

Table 2

Ultraviolet line intensities

(Unit: I_H per particle)

line	present work 100 km/sec	Raymond (1979) model C
CII 1336	1.00×10^{-1}	9.23×10^{-2}
CII] 2324	1.72×10^{-2}	9.50×10^{-2}
CIII 977	1.81×10^{-1}	1.32×10^{-1}
CIII] 1910	1.05×10^{-1}	1.03×10^{-1}
CIV 1549	5.01×10^{-3}	3.28×10^{-3}
NII 1088	1.29×10^{-2}	-
NII] 2142	1.36×10^{-2}	-
NIII 991	1.72×10^{-2}	8.55×10^{-3}
NIII] 1751	1.83×10^{-2}	-
NIV] 1485	2.99×10^{-4}	-
NV 1240	0.0	0.0
OIII] 1664	3.12×10^{-2}	1.86×10^{-2}
OIV] 1401	3.44×10^{-4}	0.0
OV] 1213	0.0	0.0
OVI 1034	0.0	0.0
SiII 1824	3.77×10^{-2}	-
SiII 1263	1.68×10^{-2}	2.58×10^{-2}
SiII] 2339	1.45×10^{-2}	-
SiIII 1198	-	3.44×10^{-2}
SiIII 1206	5.00×10^{-2}	1.42×10^{-1}
SiIII] 1887	1.81×10^{-2}	-
SiIV 1397	4.08×10^{-3}	3.82×10^{-3}

Table 3

Forbidden line intensities

(unit: I_H per particle)

line	present work 100 km/sec	Raymond (1979) model C
[OII] 3727/3729	1.74×10^{-1}	2.30×10^{-1}
[NeIII] 3868/3968	3.86×10^{-3}	3.84×10^{-3}
[SII] 4069/4076	1.57×10^{-3}	2.29×10^{-3}
[OIII] 4363	3.02×10^{-3}	3.08×10^{-3}
[OIII] 4959/5007	6.67×10^{-2}	7.55×10^{-2}
[NI] 5198/5201	1.77×10^{-3}	8.66×10^{-4}
[NII] 5755	8.26×10^{-4}	1.27×10^{-3}
[OI] 6300/6363	3.02×10^{-3}	3.33×10^{-3}
[NII] 6548/6584	2.28×10^{-2}	4.51×10^{-2}
[SII] 6717/6730	1.64×10^{-2}	2.69×10^{-2}
[OII] 7320/7330	8.72×10^{-3}	9.21×10^{-3}
[SII] 10284/10336	1.07×10^{-3}	1.34×10^{-3}
[CII] 156μ	1.02×10^{-2}	2.18×10^{-3}
[OI] 64μ	2.89×10^{-2}	3.82×10^{-3}
[NeII] 12.8μ	3.21×10^{-2}	6.55×10^{-3}

Table 4

Hydrogen line intensities and b_n values *

(shock velocity: 100 km/sec, density; 10^{-24} gcm^{-3})

		emissivity peaks			whole shock wave
		first		second	
		(T_e=7.15x10^{4}K, α_{HII}=0.561)		(T_e=5230K, α_{HII}=0.690)	
		Case A	Case B	Case B	Case B
relative line intensities	Hα	674	871	262	318
	Hβ	100	100	100	100
	Hγ	25.3	22.6	52.0	49.6
	Hδ	8.60	7.25	31.3	29.5
Hβ emissivity		16.7$^+$	30.7$^+$	100$^+$	1.77 x 10^{-2}‡
b_n values	n = 2	4.23 x 10^4	-----	-----	-----
	3	5.86 x 10^3	1.40 x 10^4	1.32 x 10^{-2}	-----
	4	2.12 x 10^3	3.88 x 10^3	4.77 x 10^{-2}	-----
	5	1.07 x 10^3	1.78 x 10^3	9.22 x 10^{-2}	-----
	6	6.37 x 10^2	9.86 x 10^2	1.38 x 10^{-1}	-----

* The reombination coefficients are from Seaton (1959a, b), and the coefficients for electronic collisions are from Kanno (see Itoh and Kogure 1967)

\+ Relavive volume emissivities at the respective points.

‡ Absolute value in unit of I_H per particle.

Captions

Fig. 1. The structure of the 100 km/sec shock model. In the upper part are given the temperatures (T: mean, T_h: heavy particle, T_e: electron) and the densities (N: heavy particle, N_e: electron). The lower part shows the ionization degree of hydrogen (α_{HII}) and the Lyman continuum flux per hydrogen (F^-: upstream, F^+: downstream).

Fig. 2. Change rate of enthalpy per electron by various processes in the 100 km/sec shock wave. The plus and minus signes denotes the gain and the loss, respectively. The processes are the elastic collisions with protons (PE) and with atoms (AE), the whole inelastic collisions with hydrogen atoms (H), the excitation of hydrogen atoms (EX), the excitations of the permitted lines (PL), the forbidden lines (FL) and the semi-forbidden lines (SF), and the interaction with Lyman continuum (LC). The rate for the last process is multiplied by a factor 100 for illustration, and the other minor processes are not shown.

Fig. 3. The ionization degrees in the 100 km/sec shock wave for elements of helium, oxgen, neon and sulfur.

Fig. 4. The distributions of the relative emissivities of the forbidden lines originating in oxgen. The shock velocity is 100 km/sec. For the absolute value, see table 3.

Fig. 5. The distributions of the relative emissivities of representative Balmer lines. The characters A and B in the parenthesis designate Case A and Case B, respectively. For the absolute value, see table 4. The shock speed is 100 km/sec.

Fig. 6. A model Balmer decrement for the interstellar shock wave (thick curves). The marked figures aside the curves are the fraction of the contribution in Hβ from the temperature relaxation region. For details of the model, see text. The recombination decrement (dashed lines) for T_e = 5000 K with the interstellar reddening is also given. The amount of the reddening is marked in E_{B-V} aside the lines. The crosses are observational results for the Cygnus Loop (1, 2, 3) and for Vela X.

Figure 1

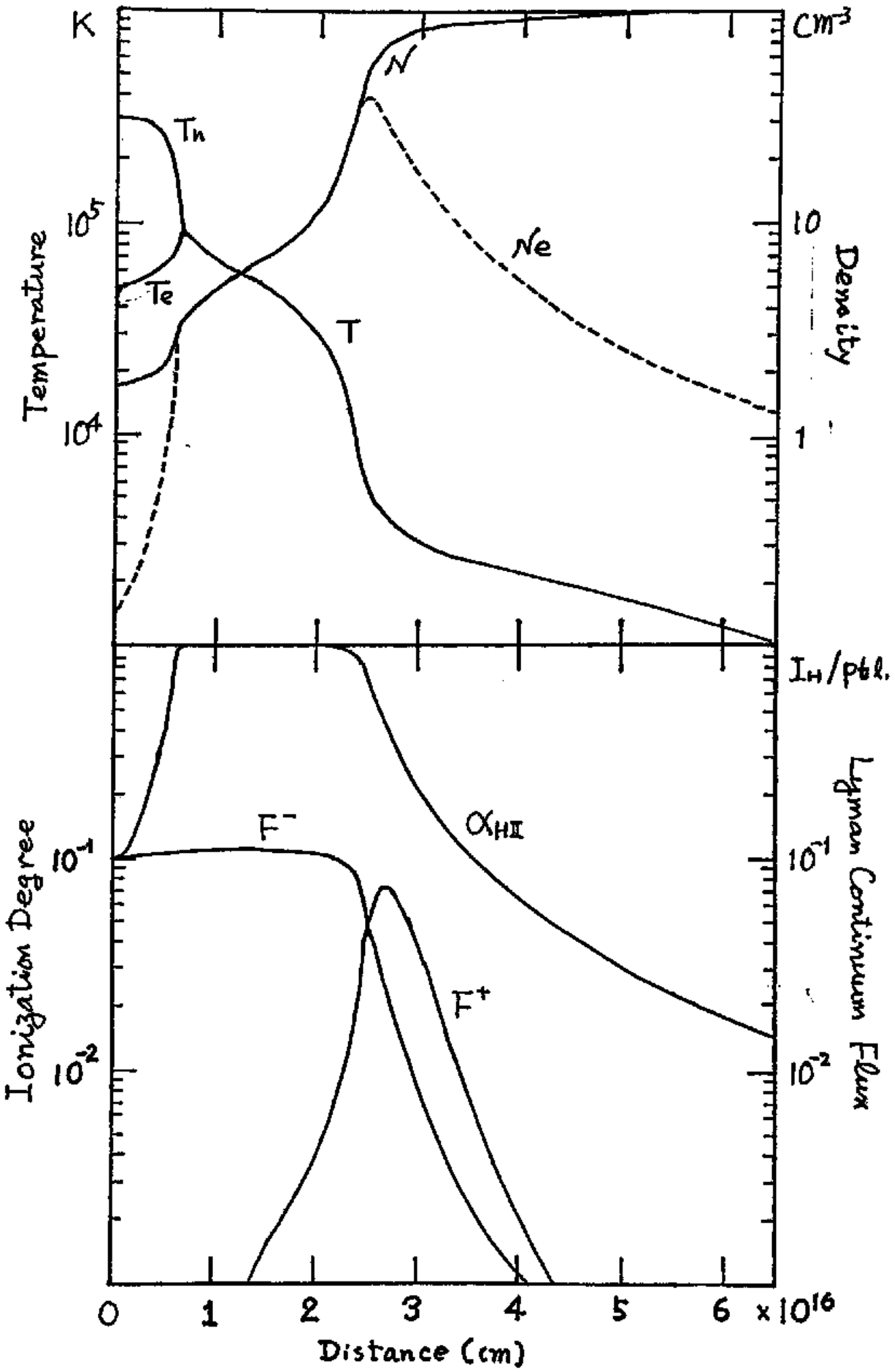
K
cm-3
N
Tn
Ne
Te
T
Temperature
Density
10^5
10^4
10
1
IH/pbl.
F-
αHII
F+
Ionization Degree
Lyman Continuum Flux
10^-1
10^-2
0
1
2
3
4
5
6
x10^16
Distance (cm)

Figure 2

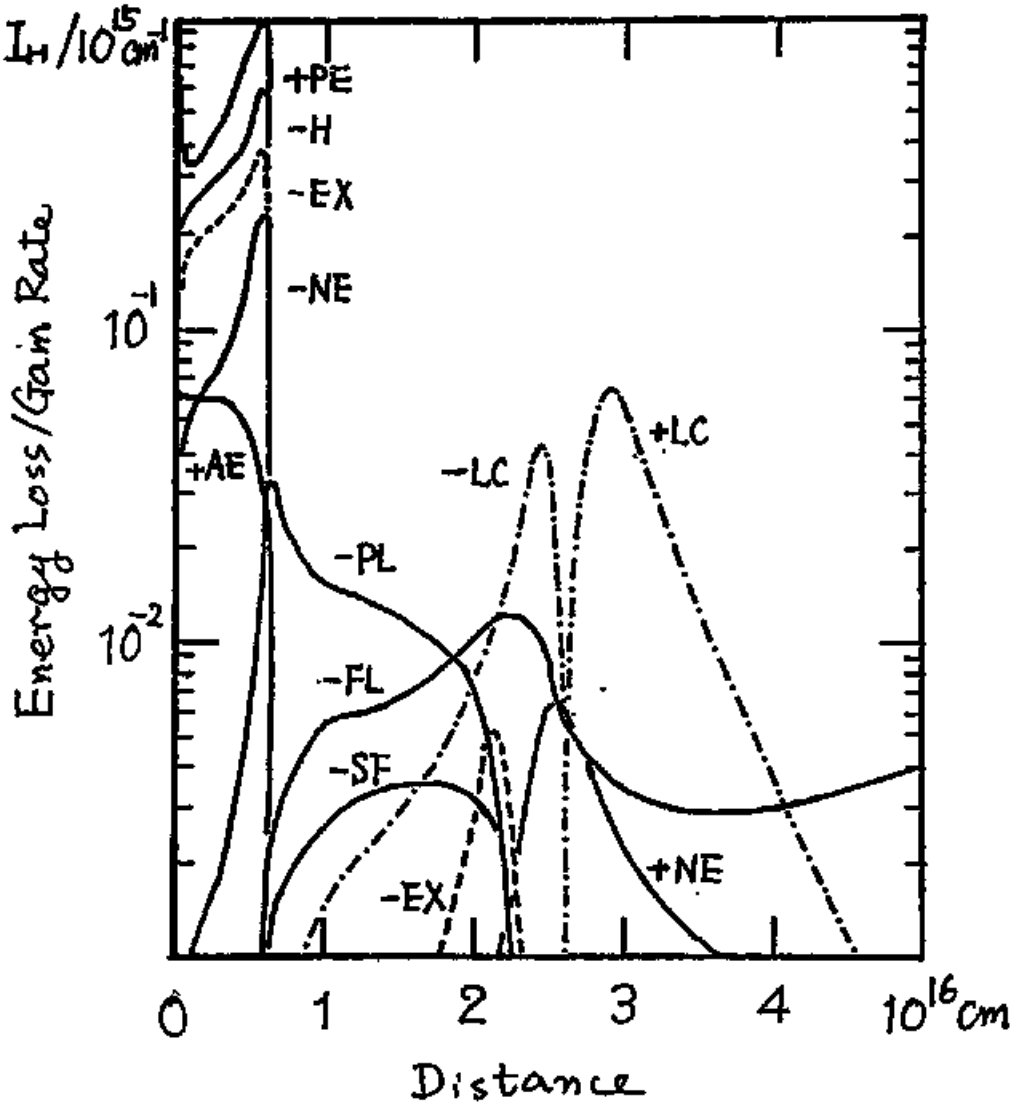
$I_H/10^{15}cm^{-1}$
Energy Loss/Gain Rate
10^{-1}
10^{-2}
+PE
-H
-EX
-NE
+AE
-LC
+LC
-PL
-FL
-SF
-EX
+NE
0
1
2
3
4
$10^{16}cm$
Distance

Figure 3

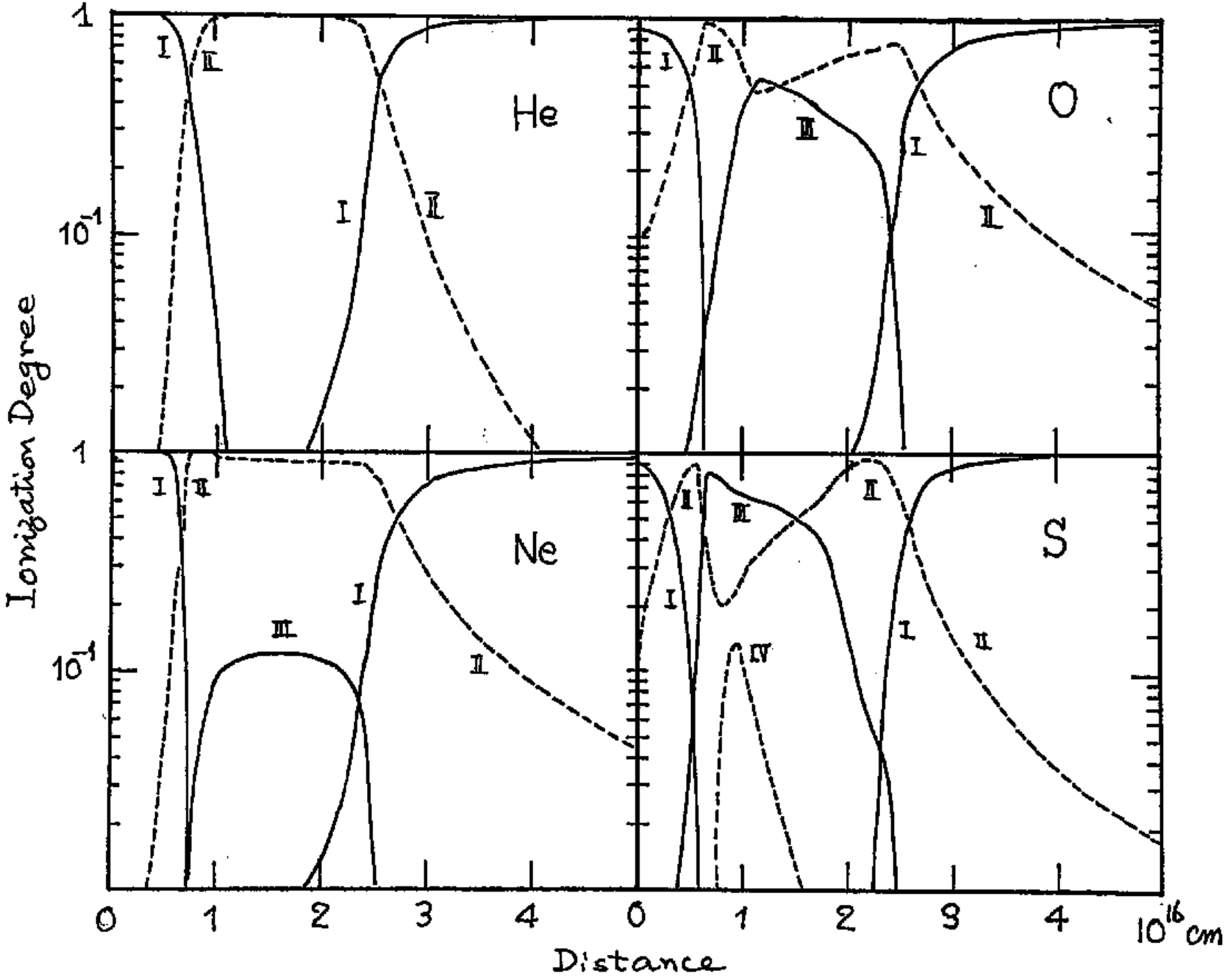
1
10^{-1}
1
10^{-1}
Ionization Degree
He
O
Ne
S
I
II
III
IV
0
1
2
3
4
0
1
2
3
4
10^{16} cm
Distance

Figure 4

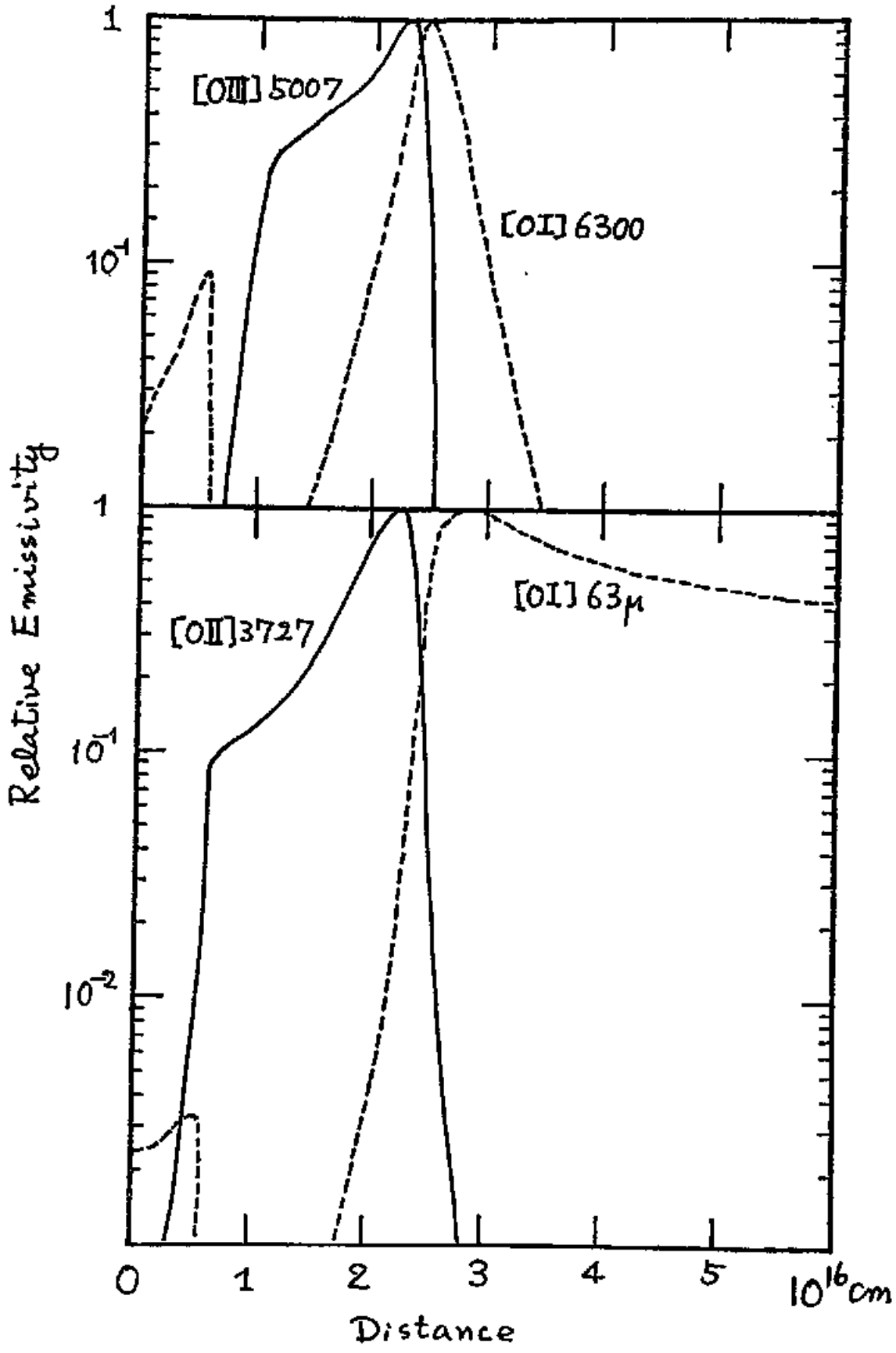
[OIII] 5007
[OI] 6300
[OII] 3727
[OI] 63μ
Relative Emissivity
1
10^{-1}
1
10^{-1}
10^{-2}
0
1
2
3
4
5
10^{16} cm
Distance

Figure 5

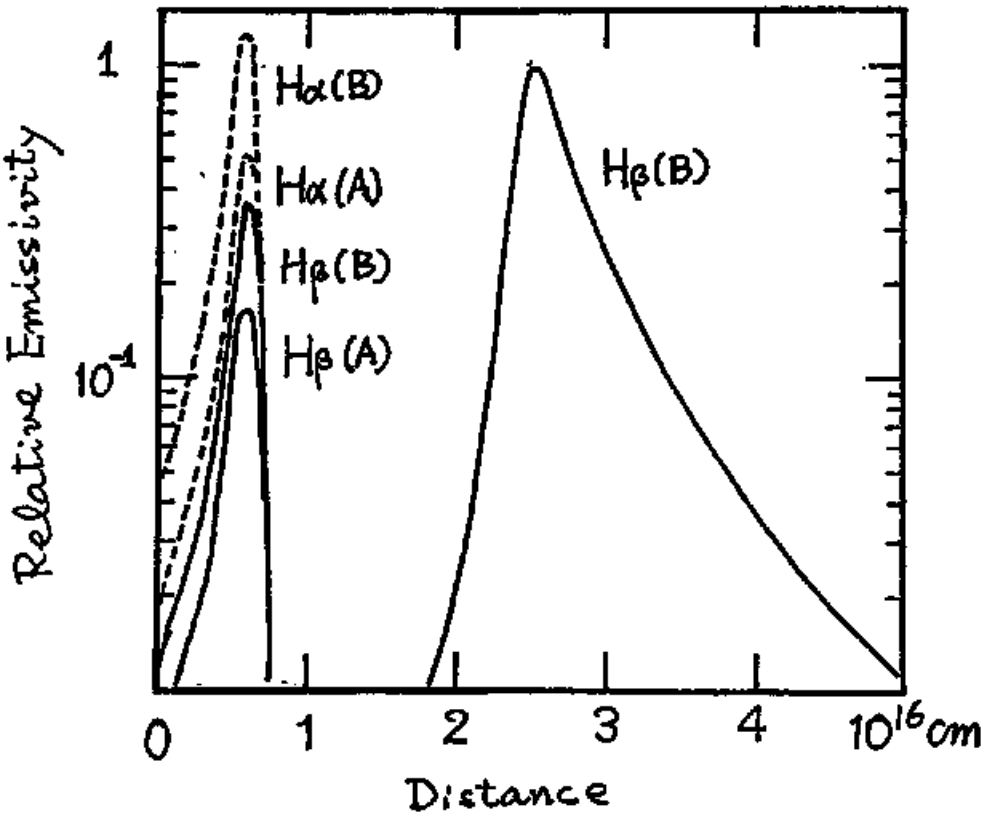
Relative Emissivity
1
10^{-1}
Hα(B)
Hα(A)
Hβ(B)
Hβ(A)
Hβ(B)
0
1
2
3
4
10^{16}cm
Distance

Figure 6

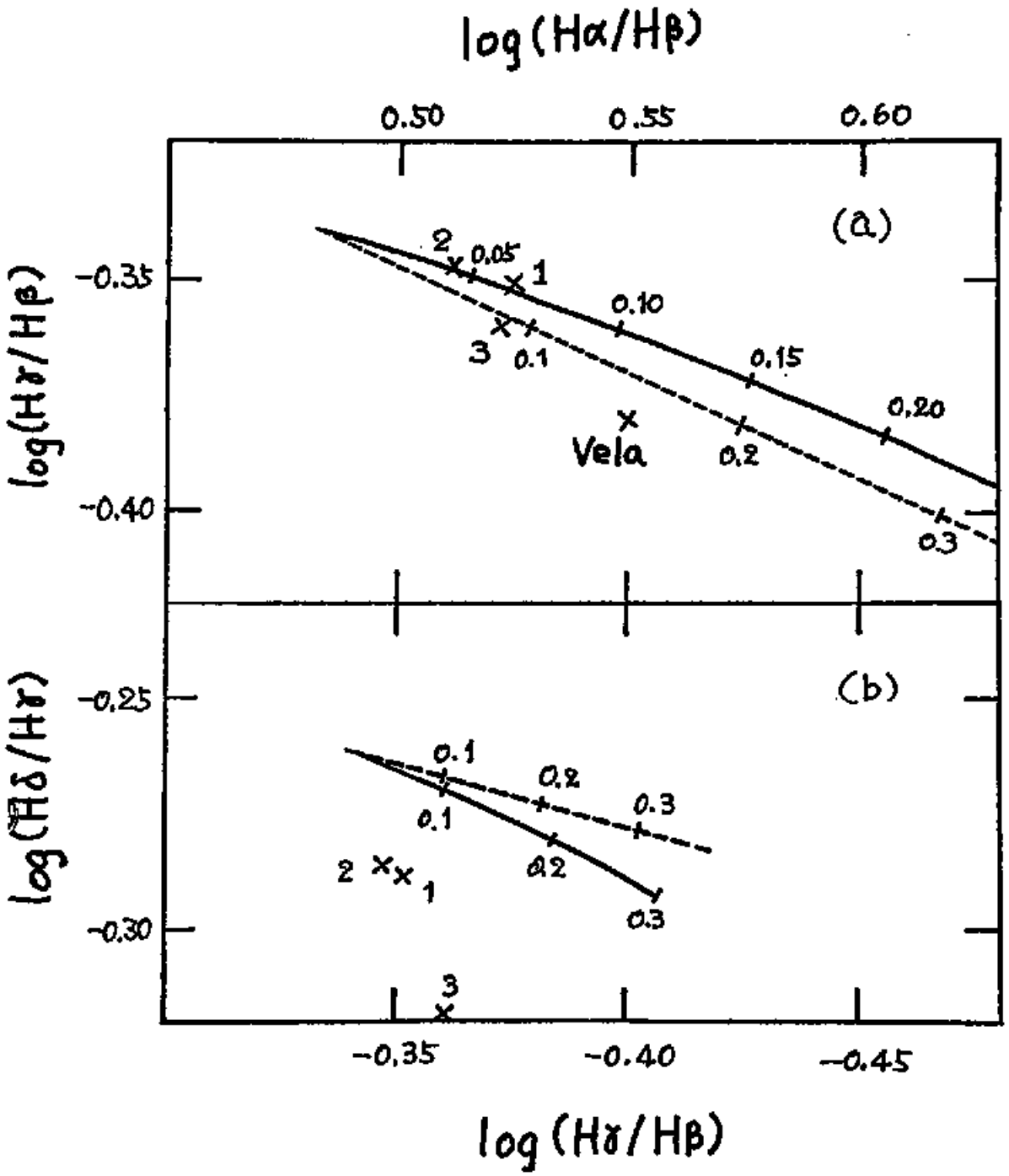
log (Hα/Hβ)
0.50
0.55
0.60
(a)
2
0.05
1
0.10
3
0.1
0.15
0.20
Vela
0.2
0.3
log(Hγ/Hβ)
-0.35
-0.40
(b)
log(Hδ/Hγ)
-0.25
-0.30
0.1
0.2
0.3
0.1
0.2
0.3
2
1
3
-0.35
-0.40
-0.45
log (Hγ/Hβ)